Synthesis and properties of carbon microspheres based on tannin-sucrose mixtures treated in hydrothermal conditions

Angela Sanchez-Sanchez, Flavia L. Braghiroli, M.T. T Izquierdo, Julien Parmentier, Alain Celzard, V. Fierro

Synthesis and properties of carbon microspheres based on tannin-sucrose mixtures treated in hydrothermal conditions

A. Sanchez-Sanchez[1], F.L. Braghiroli[1,2], M.T. Izquierdo[3], J. Parmentier[4], A. Celzard[1], V. Fierro[*1]

[1] Université de Lorraine, CNRS, IJL, F-88000 Epinal, France

[2] Centre Technologique des Résidus Industriels (CTRI), Cégep de l'Abitibi-Témiscamingue, 425 Boul. du Collège, Rouyn-Noranda, QC J9X 5E5, Canada

[3] Instituto de Carboquímica, ICB-CSIC, Miguel Luesma Castán, 4. 50018 Zaragoza, Spain

[4] Université de Haute Alsace, Institut de Science des Matériaux de Mulhouse, LRC CNRS 7228, 15 rue Jean Starcky, BP 2488, 68057 Mulhouse Cedex, France

[*] Corresponding author. Tel: + 33 329 29 61 77. Fax: + 33 329 29 61 38. E-mail address : Vanessa.Fierro@univ-lorraine.fr (V. Fierro)

Abstract

Sustainable carbon materials have been synthesised by use of inexpensive natural precursors, tannin and sucrose, mixed in aqueous solution in various proportions (from 0:1 to 1:0), and then submitted to hydrothermal carbonisation (HTC) at various pH (from 2 to 8) and temperatures (160, 180 or 200°C). The resultant hydrochars were finally pyrolysed at 900°C under nitrogen flow to produce highly porous carbon materials with BET areas as high as 810 m^2/g without activation. The effects of the initial tannin/sucrose weight ratios and of the HTC conditions were investigated in terms of final particle size (from 1 to 10 µm), carbon yield (from 30 to 45%), composition (C from 88 to 93 wt. %; O from 6 to 10 wt. %), surface chemistry (C from 88 to 98 at. %; O from 2 to 12 at. %) and porous texture (NLDFT surface areas and micropore volumes from 840 to 1420 m^2/g and from 0.23 to 032 cm^3/g, respectively). All these parameters were discussed and correlated with the electrochemical properties of the same materials. Special attention was paid to the separate roles of porosity and surface chemistry, and on the reversibility of the electrochemical reactions.

Keywords: Tannin; Sucrose; Hydrothermal Carbonisation; Sustainable Carbons; Supercapacitor electrodes.

1. Introduction

Carbon materials are applied to several fields of paramount importance such as catalysis, water and air depollution, and energy storage and conversion such as secondary batteries or supercapacitors. The production of "sustainable carbon materials" from inexpensive carbon sources including lignocellulosic biomass or other by-products contained in food/agricultural waste, is of major importance nowadays. One way of achieving this target and producing functionalised carbon materials is applying hydrothermal carbonisation (HTC) as a low-cost, scalable, and industrially attractive first step of carbonisation prior to pyrolysis (Antonietti and Titirici, 2010; Celzard et al., 2012; Hu et al., 2010). HTC maintains high oxygen content and allows the functionalisation of the resultant materials without the need of additional chemical reagents (Unur, 2013). The use of moderate temperature and pressure conditions are fundamental for the onset of several reactions to which carbohydrates are submitted such as hydrolysis, dehydration, condensation, aromatisation and polymerisation (Sevilla and Fuertes, 2009). An insoluble black solid that contains higher carbon content than in the original material is obtained, and then a second-step of pyrolysis at 900°C can be applied for increasing the electrical conductivity and improving the textural properties of the final materials.

HTC has been applied to a broad range of carbohydrates and biomass: rice grains, oak leaves, pine needles (Titirici et al., 2007), microalgae (Falco et al., 2012) and prawn shells (White et al., 2009). Mimosa tannin has also been submitted to HTC. Mimosa tannin is a phenolic material that has been used for the production of several materials such as resins/adhesives (Pizzi, 1994), foams (Tondi et al., 2009; Letellier et al., 2017), gels (Szczurek et al., 2011a, 2011b) and recently N-doped carbon materials (Braghiroli et al., 2012, 2015a). This is explained by the fact that such condensed (flavonoid) tannins are quite reactive in the presence of aldehydes (e.g. formaldehyde), and another advantage is that they

can auto-condensate, especially when heated or in presence of strong mineral acids (Pizzi, 1983). Fig. 1 shows the main flavonoid structure of the robinetinidol unit (resorcinol A-ring and pyrogallol B-ring) which constitutes approximately 70% of Mimosa tannin extract (Bate-Smith, 1962; Pizzi, 1983; Hemingway et al., 1989; Pizzi, 1994).

Figure 1

Various carbonaceous microspheres were obtained after tannin HTC, depending on temperature, reaction time and tannin concentration, and their production was found to obey a first-order kinetics with an activation energy of 91 kJ mol^{-1} (Braghiroli et al., 2014). The mechanism of microspheres formation proceeds by nucleation, leading to a high number of small particles, followed by growth and coalescence, leading to bigger particles of lower surface area. The hydrochar yield investigated as a function of pH was found to increase from 64.4 % at unmodified pH (around 4.2 for the aqueous tannin solution) to 86.7 % when the pH was decreased to 1. The pH also influenced the morphology and the texture of the hydrochars, those prepared at non-modified pH being powders, whereas those obtained at low pH being stiff monoliths presenting a higher surface area, up to 800 m^2 g^{-1} after pyrolysis at 900°C. But in all cases, the micropore size distributions were the same (Braghiroli et al., 2015b).

Concerning sugars, Wang et al. (2001) submitted a sucrose solution (1.5 mol L^{-1}) to HTC at 190°C during 5h to produce carbonaceous microspheres with an average diameter of 5 µm and a BET area as high as 400 m^2 g^{-1} after subsequent pyrolysis at 1000°C. Then, Sevilla and Fuertes (2009) studied the hydrochars obtained after HTC of several saccharides in different conditions of temperature (170-240°C) and reaction time (0.5-15h) concluding that they presented a core–shell structure consisting of a hydrophobic core and a hydrophilic shell containing reactive oxygenated functional groups. Next, Falco et al. (2012) observed the effect of adding glucose to microalgae organisms submitted to HTC, and found that such

strategy allowed incorporating nitrogen in the final carbon matrix and also increasing the carbon yield from 18 to 47.5%.

In the present study, we used condensed tannin combined with commercial sugar (sucrose) to see the effects of such mixture on the preparation of carbon materials. Sucrose was selected because it is a commercial product, readily available and not expensive but also for comparison purposes with previous studies (Wang et al., 2001; Sevilla and Fuertes, 2009). Various kinds of microspheres were seen by electron microscopy, depending on temperature, pH, and sucrose / tannin ratio. After a subsequent thermal treatment at 900°C, the final carbon materials presented developed textural properties especially at low pH. To understand better the influence of the various chemical and structural characteristics of the present carbons, some of them were tested as electrode materials and the reversibility of the oxygen groups' reactions in acidic electrolyte was studied. Such electrochemical studies allowed separating the roles of the materials' features, and suggesting how to improve further their capacitance if we were to start developing supercapacitor electrodes.

2. Materials and methods

2.1 Raw materials

Mimosa tannin, kindly supplied by SilvaChimica, was used in this study. The extraction process and the composition of the tannin extract was described elsewhere (Braghiroli et al., 2014).

2.2 Hydrothermal treatment

In a typical synthesis, 2.0 g of either tannin (T) alone, sucrose (S) alone, or tannin-sucrose mixture, were dissolved in 16.0 g of water, put inside a glass vial and then into a Teflon-lined autoclave for 24h installed in an oven preheated at 180°C. Different conditions of hydrothermal carbonisation (HTC) were studied, using various fractions of sucrose: 0, 25, 50,

75 and 100 wt. %. The addition of sucrose changed the pH from 4.2 (100% T) to 8 (100% S). The resultant materials were called HsStT180_u, s and t being the percentages of sucrose and tannin, respectively, and u meaning unmodified pH. A second series of samples was prepared by fixing the pH at 2 by use of pTSA. Those materials were labelled HsStT180_2. The HTC temperatures were also varied, 160 or 200°C, and the corresponding samples were labelled HsStT160_u or HsStT200_u for unmodified pH experiments.

In all cases, the filtrates were recovered, washed with water, and then dried in a vacuum oven at 80°C. Pyrolysis was carried out under nitrogen flow in a tubular furnace heated at 1°C min^{-1} up to 900°C, and this temperature was hold for 3h. Pristine tannin (0S100T) was also carbonised in the same conditions and labelled C0S100T. In order to distinguish carbon materials from hydrochars, we added a 'C' at the beginning of the label; for instance, the sample H100T180_2 became CH100T180_2 after pyrolysis at 900°C.

2.3 Materials characterisation

Scanning electron microscopy (SEM) observations were carried out with a FEI-Quanta 400 apparatus for investigating the morphology of the samples, which were metallised beforehand. A series of images was taken for each sample, and only one was provided here as an example. The purpose was to evaluate the morphology of the samples and to observe general trends in the particle size, depending on the preparation conditions.

Pore texture parameters were obtained by krypton adsorption at -196°C for organic, or non-porous samples obtained after HTC, and by nitrogen adsorption at -196°C for pyrolysed materials, using a ASAP 2020 automatic apparatus (Micromeritics) in both cases. CO_2 adsorption at 0°C was also carried out on pyrolysed samples using a Micromeritics ASAP 2420 apparatus. The following parameters were determined: NLDFT surface area, S_{NLDFT} (m^2 g^{-1}); BET area, A_{BET} (m^2 g^{-1}); total pore volume, $V_{0.97}$ (cm^3 g^{-1}); micropore volumes, $V_{DR,N2}$

and $V_{DR,CO2}$ (cm^3 g^{-1}), from the N_2 or CO_2 adsorption isotherms; micropore volume, $V_{\mu,NLDFT}$ (cm^3 g^{-1}), by applying the 2D- NLDFT-HS to both CO_2 and N_2 adsorption isotherms; and mesopore volume, V_{mes} (cm^3 g^{-1}), calculated as the difference $V_{0.97} - V_{DR,N2}$. The pore size distributions (PSDs) were calculated by applying the 2D-NLDFT-HS method to both CO_2 and N_2 adsorption isotherms. More details are given elsewhere (Schaefer et al., 2016).

Ultimate analyses of samples were carried out in a CHONS elemental analyser (Vario El cube, Elementar) as reported elsewhere (Celzard et al., 2019). Temperature-Programmed Desorption (TPD) experiments were performed with a custom-built set-up, consisting of a tubular quartz reactor placed inside an electric furnace. In a typical experiment, the sample was heated up to 1100°C in Ar atmosphere at a heating rate of 10°C min^{-1}. The amounts of CO and CO_2 were determined as reported elsewhere (Tellez-Juárez et al., 2014).

X-ray photoelectron spectroscopy (XPS) results were recorded with an ESCAPlus OMICROM system equipped with a hemispherical electron energy analyser. Measurements were carried out as reported elsewhere (Sanchez-Sanchez et al., 2018).

Electrochemical characterisation was performed with a Biologic VMP3 multi-potentiostat. The carbon electrodes were prepared by spreading onto a graphite foil a paste (~15 mg cm^{-2}) made of the carbon material mixed with polytetrafluoroethylene (PTFE) binder and carbon black in the weight percent ratio of 85:10:5. The resulting electrodes were then pressed at 5 MPa and impregnated by 1 mol L^{-1} H_2SO_4 electrolyte during 48 hours. Cyclic voltammetry (CV) tests were carried out at different scan rates between 0.5 and 100 mV s^{-1} and within the potential window of 0 – 0.8 V in a three-electrode cell, using a platinum gauze as the counter electrode and a saturated calomel electrode (SCE) as the reference one. The specific capacitance (C, F g^{-1}) was calculated form the CV curves according to Eq. (1):

$$C = (\int I\, dV) / (s\, \Delta V\, m) \quad (1)$$

where I (A) is the current, s (V s^{-1}) is the scan rate, ΔV (V) is the potential window and m (g) is the mass of carbon in the electrode.

3. Results and discussion

3.1 Carbon yields and morphologies

To study the effects of the pH on the tannin / sucrose solution submitted to HTC, the same weight (1 g) of sucrose and tannin was used. Table 1 shows the main characteristics of these hydrochars (H50S50T) at different pH ranging from 1 to unmodified (4.2). Unlike H0S100T (100% tannin submitted to HTC - see Fig. 2), submitting 50S50T to HTC at different pH did not produce any change in the HTC yield. Being at the level of 61.5 ± 1.5 wt. %, the HTC yield of 50S50T was also always much lower than that of H0S100T. The A_{BET} values (around 1 m^2 g^{-1}) were almost the same for 0S100T, H0S100T and H50S50T, considering the intrinsic uncertainties of adsorption techniques as soon as very low surface areas are concerned. Therefore, it can be concluded that, after HTC, the materials were not porous.

After a second thermal treatment at 900°C, A_{BET} increased from 471 m^2 g^{-1} for tannin directly pyrolysed (C0S100T) to 639 m^2 g^{-1} for CH50S50T 180_u (i.e., at unmodified pH), and even up to 809 m^2 g^{-1} for CH50S50T 180_1 (i.e., at pH 1). The increase of A_{BET} was also observed for the 100% tannin material (CH0S100T) having been submitted to HTC at low pH. Fig. 2 summarises the results of HTC yield and A_{BET} of all these hydrochars H0S100T and CH0S100T (already demonstrated in (Braghiroli et al., 2015b)) and H50S50T and CH50S50T at pH values ranging from 4 to 1. The results on pure tannin are presented here for the sake of comparison to study the effect of sucrose addition.

Figure 2

It has already been mentioned that heating tannin in the presence of strong mineral acids favours its condensation/polymerisation reactions by different possible ways to form "phlobaphenes" or "tanner's reds", which are high-molecular weight, insoluble molecules (Pizzi, 1983; Braghiroli et al., 2015a). Tannin treated after HTC at 180°C was shown to have

193 a structure similar to that of flavonoid tannin (see Fig. 1), but presents a much higher level of
194 polymerisation, mainly through the opening of the heterocyclic C2–ring and subsequent
195 partial condensation between C2 (open) to C6 or C8, and partly through some auto-
196 condensation C4 to C6 and C8 (Braghiroli et al., 2015a).

197 On the other hand, sucrose submitted to HTC undergoes hydrolysis that produces glucose
198 and fructose, which decompose into hydroxymethylfurfural (HMF) as the main dehydration
199 product, plus aldehydes (formaldehyde, pyruvaldehyde, etc.) and organic acids (acetic,
200 formic, levulinic acids, etc.), hence producing a rapid pH change from 8 to 3 as shown in the
201 literature (Antal et al., 1990; Ulbricht, 1984; Asghari and Yoshida, 2006). Glucose and
202 fructose can also undergo polymerisation and condensation reactions as reported elsewhere
203 (Antal et al., 1990; Kabyemela et al., 1997; Luijkx et al., 1995; Sevilla and Fuertes, 2009).
204 Titirici et al. (2008) observed that the morphologies and chemical structures of carbons
205 obtained from sucrose are directly related to those of carbons obtained from pure furan. It was
206 also found that such intermediate molecules derived from saccharide dehydration as
207 mentioned above coexist with furans and account for the observed changes of particle size,
208 textural properties and particles aggregation.

209 When both materials (tannin and sucrose) coexist, we can assume that several reactive
210 germs are obtained through hydrolysis of sucrose submitted to HTC. SEM photos show that
211 the average microsphere diameter was reduced from 10 µm for H0S100T (see Fig. 3a) to 2-5
212 µm by simple addition of sucrose (see Fig. 3c) for H50S50T, whereas 100% sucrose produced
213 spheres of average size 1-2 µm (see Fig. 3b). This finding suggests that sucrose reacts faster
214 than tannin, producing more germs and, consequently, smaller spheres are obtained (see Fig.
215 3c).

216

217 Table 1: Textural properties and elemental analysis obtained for materials 50S50T after HTC and subsequent pyrolysis made at different pH.

		Yield (wt. %)			Textural Properties						Elemental Analysis (wt. %)					
	Sample	HTC	Carbon	Total	S_{NLDFT} ($m^2 g^{-1}$)	A_{BET} ($m^2 g^{-1}$)	$V_{0.97}$ ($cm^3 g^{-1}$)	$V_{DR,N2}$ ($cm^3 g^{-1}$)	$V_{DR,CO2}$ ($cm^3 g^{-1}$)	$V_{\mu,NLDFT}$ ($cm^3 g^{-1}$)	C	H	N	S	O	C/O
No HTC	**0S100T**	-	-	-	-	0.27	-	-	-	-	53.8	5.4	0.6	0.1	40.1	1.3
After HTC	**H0S100T180_u**	64.6	-	-	-	0.78	-	-	-	-	60.9	4.4	0.8	0.0	33.8	1.8
	H50S50T180_1	63.0	-	-	-	1.22	-	-	-	-	62.6	5.0	0.6	0.2	31.6	2.0
	H50S50T180_2	60.0	-	-	-	1.05	-	-	-	-	62.6	4.3	0.2	0.2	32.7	1.9
	H50S50T180_3	61.2	-	-	-	0.87	-	-	-	-	62.3	4.8	0.8	0.0	32.1	1.9
	H50S50T180_u	61.5	-	-	-	0.84	-	-	-	-	60.9	4.4	0.3	0.0	34.4	1.8
	H100S0T180_u	41.1	-	-	-	1.8	-	-	-	-	65.6	4.4	0.0	0.0	30.0	2.2
After pyrolysis at 900°C	**C0S100T**	-	44.5	44.5	1416	471	0.20	0.19	0.38	0.32	90.4	0.8	0.6	0.0	8.2	11.0
	CH0S100T180_u	64.6	51.6	33.4	904	608	0.24	0.23	0.28	0.25	88.3	0.9	0.6	0.0	10.2	8.7
	CH50S50T180_1	63.0	50.4	31.8	1132	809	0.35	0.31	0.36	0.32	89.9	1.5	0.8	0.0	7.8	11.5
	CH50S50T180_2	60.0	53.2	31.9	1061	767	0.34	0.29	0.32	0.30	91.5	1.1	1.2	0.0	6.2	14.8
	CH50S50T180_3	61.2	48.4	29.6	984	643	0.27	0.25	0.29	0.27	90.8	2.1	0.8	0.0	6.3	14.4
	CH50S50T180_u	61.5	49.6	30.5	913	639	0.25	0.24	0.28	0.25	91.0	0.5	0.3	0.0	8.2	11.1
	CH100S0T180-u	41.1	51.2	21.1	836	562	0.22	0.22	0.26	0.23	93.0	0.5	0.1	0.0	6.4	14.5

218

A similar effect was found by decreasing the pH down to 2. Small spherical particles of around 2 µm arranged in a necklace structure were indeed obtained in carbons based on either pure tannin (see Fig. 3d) or tannin-sucrose mixture (compare Fig. 3c, 3f, 3g and 3h) submitted to HTC at pH 2. No changes in particle diameter were observed, as their size was nearly constant around 2 µm, irrespective to the HTC temperature: 160, 180 or 200°C. This finding at lower pH is different from what was formerly observed for H0S100T at unchanged pH and 160°C, for which irregular spheres were found, indicating that HTC reaction was not finished. By increasing the HTC temperature from 180 to 200°C, bigger and rounded spheres were observed (Braghiroli et al., 2014).

Figs. 3b and 3e show SEM pictures of carbon materials derived from 100S0T submitted to HTC at unchanged pH (pH around 4) or at pH 2. HTC of 100S0T at unchanged pH produced mostly monodisperse spherical particles having a size of approximately 1 µm, in agreement with other authors (Titirici et al., 2008; Sevilla and Fuertes, 2009). However, sucrose hydrolysis at pH 2 produced bigger spheres of around 5-10 µm. Zhao et al. (2013) observed the effect of the acidic pH on the formation mechanism of carbon spheres when submitting cellulose to HTC. The compounds obtained from cellulose hydrolysis rapidly react with H^+ present in the system through dehydration and polymerisation reactions and lead to hydrochar nucleation. Besides that, they concluded that the acid concentration in the HTC system could also control the shape and the diameter of the carbon spheres.

Figure 3

Table S1 shows the main characteristics of hydrochars and carbon materials prepared with 50% of sucrose (50S50T) at different HTC temperatures (160, 180 and 200°C) and different pH. Some of these results are summarised in Fig. 4 including the total carbon yield and the A_{BET} as a function of HTC temperature at unchanged pH or at pH 2. The HTC yield was around 60% irrespective to the temperature or the pH. After pyrolysis, the total carbon yield

appears to be constant, around 30%, whatever the HTC temperature or the pH used beforehand. In the same way, A_{BET} did not change with HTC temperature but was higher for samples prepared at pH 2. Indeed, carbons prepared from hydrochars obtained at pH 2 presented an A_{BET} of 735 ± 32 $m^2 g^{-1}$, while those prepared at unchanged pH had an A_{BET} of 629 ± 10 $m^2 g^{-1}$.

Figure 4

In order to study the effect of the percentage of sucrose on the hydrochar characteristics, hydrochars based on various proportions of tannin and sucrose were prepared at unchanged pH and at pH 2, summarised in Table S2. We can observe by SEM photos in Fig. 5a to 5c that, by increasing the weight fraction of sucrose from 25 to 100% at unchanged pH, the sphere diameter decreased from around 10 to 2 µm and they became more individualised and more monodispersed. Polydispersity and higher particle size thus appear to be a consequence of tannin presence in the system at unchanged pH. In the literature, changes of particles morphology produced by mixing two carbon precursors submitted to HTC were also evidenced for microalgae in the presence of glucose added in a mass ratio of 1:1. In that case, the final particles morphology was that of pure glucose but with a double higher average diameter, passing from 1 to 2 µm (Falco et al., 2012). Coming back to the present situation, the effect of adding sucrose at pH 2 was opposite to that observed at unchanged pH. With the addition of sucrose at lower pH, the average sphere diameter increased from 1-2 µm to 2-3 µm and finally to around 5-10 µm when the proportion of sucrose increased from 25% (Fig. 5d), to 75% (Fig. 5d) until 100% (Fig. 5f), respectively.

Figure 5

Fig. 6a shows the HTC yield of all materials at different proportions of sucrose / tannin and at two pH, unchanged and 2. The dotted lines represent the theoretical yield calculated from

the experimental yields of 0S100T and 100S0T (e.g. for 75S25T we have $Y_{HTC,\ 75S25T}$ = (75 × $Y_{HTC,100S0T}$ / 100 + 25 × $Y_{HTC,0S100T}$ / 100), in order to observe any synergetic effect between tannin and sucrose during HTC. At pH 2, the experimental HTC yield was very similar to the expected value, so we can conclude that there is no apparent interaction between sucrose and tannin regarding the yield. Acidic pH accelerates HTC reactions, both for sucrose and tannin precursors (Lee et al., 1999; Kim et al., 2001; Trajano and Wyman, 2013) and no differences were observed. At unmodified pH, experimental HTC yield of tannin-sucrose mixtures were higher than those theoretically calculated, suggesting that HTC products of sucrose and tannin interact with each other. At pH around 4, sucrose yielded more solid materials. Its higher HTC kinetics compared to tannin led to more germs with a resulting lower particle size and an enhanced HTC yield. Since at pH 2 the experimental HTC yield was the same as calculated, it can be assumed that a low pH promotes fast reactions to liquid products (Lee et al., 1999; Kim et al., 2001; Trajano and Wyman, 2013) that do not interact with tannin.

Figure 6

3.2 Porous texture and composition

Fig 6b shows the BET area of the same hydrochars as in Fig. 6a but after pyrolysis at 900°C. As a general remark, the addition of sucrose to tannin slightly increased A_{BET}. The highest A_{BET} was found for the mixture 50S50T at both pH, but the main effect on the increase of surface area was due to the pH reduction. Fig. 7 shows that the product A_{BET} × total carbon yield increased with the total carbon yield. This effect is opposite to what is obviously found for carbon activation, whether physical or chemical, which produces higher surface area when the carbon yield decreases, i.e., when the burn-off increases. Besides, by increasing the proportion of tannin mixed with sucrose in HTC conditions, an increase of the total carbon yield can be seen. However, the highest A_{BET} was obtained at equal proportion (50:50) of T and S at pH 2. Such increase of surface area, from 476 to 791 $m^2\ g^{-1}$, cannot be explained by

293 the decrease of particle diameter from 10 µm (CH0S100T180_u) to approximately 2 µm
294 (CH50S50T180_2), which accounts for less than 1% of the measured A_{BET}. As previously
295 discussed in Braghiroli et al. (2015b), the decrease of particle size might facilitate the
296 evolution of volatile matter and then the development of textural properties.

297 Figure 7

298 All materials were found to be microporous, given their Type I nitrogen isotherms at -
299 196°C, having a vertical part at low relative pressure P/P_0 and an almost horizontal part from
300 P/P_0 = 0.02 to 1 as shown in Fig. 8a for CH50S50T180_2 and CH50S50T180_u. The pore
301 size distribution calculated by NLDFT is presented in Fig. 8b for the same samples;
302 CH50S50T180_2 had some porosity in the mesopore range (between 2 and 10 nm), whereas
303 CH50S50T180_u presented an entirely microporous structure. The isotherm of sample
304 prepared at pH 2 presented a slight slope showing the presence of pores broader than 2 nm.
305 Most of the carbohydrates submitted to HTC needed a second thermal treatment, at higher
306 temperature, to increase the porosity of the resultant carbon materials. However, glucose after
307 HTC and subsequent pyrolysis at 900°C was poorly porous and had low surface areas, around
308 30-50 $m^2\ g^{-1}$ (Zhao et al., 2010). Thanks to the reactivity of tannins in hydrothermal
309 conditions and posterior pyrolysis at 900°C, highly porous material were obtained (A_{BET} > 600
310 $m^2\ g^{-1}$) confirming its potential as precursor for the production of porous carbons.

311 Figure 8

312 As for the chemical composition, Fig. 9a shows the van Krevelen diagram for all
313 hydrochars and carbon materials prepared from tannin and sucrose at different pH and HTC
314 temperatures (160, 180 and 200°C). The main arrow (from 100S0T to HTC_900°C, i.e., from
315 pure sucrose to all carbons obtained by HTC followed by pyrolysis at 900°C) indicates the
316 loss of oxygen and hydrogen, and therefore the increase of carbon content after both thermal
317 treatments (HTC at 160-200°C and pyrolysis at 900°C) (van Krevelen, 1950). The percentage

of carbon increased after HTC and obviously even more after pyrolysis. After HTC, samples prepared at unmodified pH retained more oxygen, 30-36 wt. %, than those prepared at pH 2, 28-33 wt. %. After pyrolysis at 900°C, carbon derived from hydrochars prepared at unmodified pH retained more oxygen, 6-10 wt. %, than those prepared at pH 2, 3-6 wt. %.

Fig. 9b shows the total amounts of CO and CO_2 gases in mmol g^{-1} that have been lost during a thermal treatment (TPD analysis) up to 1100°C for materials at different T/S proportions. CO_2 derives from precursors comprising carboxylic acids, lactones and anhydride groups, and CO derives from quinonic and phenolic groups (Figueiredo et al., 1999). Boudouard equilibrium also takes place, modifying the CO/CO_2 ratio. The total amount of released gases ($CO + CO_2$) was higher for materials HsStT_u prepared without pH modification (0.065-0.075 mmol g^{-1}) than for HsStT_2 prepared at pH 2 (0.036-0.052 mmol g^{-1}). This is in good agreement with their higher amount of oxygen, 32.4-36.3 wt. %, compared to 30.6-32.7 wt. % in HsStT_2 materials, measured by EA (Table 1 and Table S1). Indeed, tannin in the presence of strong acids undergoes dehydration and condensation reactions (Pizzi, 1983; Braghiroli et al., 2015a), which might have reduced the amount of oxygen in hydrochars.

Figure 9

Surface atomic concentrations obtained by XPS and contributions to the C1s, O1s and N1s high-resolution spectra of the hydrochars and carbon materials are collected in Table 2 and in Fig. S1 to S6 of the Supporting Information section. Tannin–derived hydrochars presented high oxygen surface concentrations, between 12.6 and 19.6 at. %, but low nitrogen surface concentrations, between 0.3 and 1.3 at. %. No influence of the pH of the medium on the oxygen surface concentration of the hydrochars was evidenced. Sucrose–derived hydrochars contained 17.9 at. % surface oxygen, and a small concentration of nitrogen, 0.3 at. %, in agreement with the chemical composition of sucrose and with the presence of amino-acids

coming from the raw sugar beet. As expected, the oxygen concentration of the hydrochars significantly decreased after pyrolysis, and the resultant carbons exhibited oxygen surface concentrations between 2.3 and 11.7 at. %. The concentration of nitrogen varied in the range 0.40 – 1.7 at. %, being only present at the surface of carbons prepared at pH higher than 3.

Deconvolution of the high-resolution XPS spectra allowed identifying chemical bonds that are characteristic of specific functional groups. C1s high-resolution spectra for all samples exhibited an asymmetric peak centred on binding energies (BE) of 284.4 – 284.5 eV (Table 2, and Fig. S1 and S4 in the Supporting Information section). Except for H50S50T180_3, the deconvolution of the C1s high-resolution profiles gave rise to five peaks, CI to CV, with binding energies (BE) between 284.4 and 290.6 eV: CI is assigned to Csp^2 in hydrocarbons, aromatics and aliphatics; CII is associated with Csp^3 and C-O single bonds associated with ethers, phenols and anhydrides; CIII is assigned to C=O double bonds in carbonyls and quinones; CIV corresponds to C-O single bonds in carboxylic groups; and CV is related to plasmon losses or shake-up π-π satellites. In the case of H50S50T180_3, an additional peak C* appeared at an unusually low BE, 283.6 eV. This peak may be associated to pre-graphite-like C in highly aromatic materials (Cagniant et al., 1998; Weckhuysen et al., 1998).

The O1s high-resolution spectra of the hydrochars presented, in general, two oxygen contributions (Table 2): O1, assigned to C=O double bonds in quinone-type groups, carbonyls and carboxylic acids; and O2, related to –OH bonds in phenols, C–O–C in ether groups and C=O bonds in ester and anhydride groups. The O1s high-resolution spectra exhibited generally O1, O2 and O3 contributions, O3 being assigned to chemisorbed oxygen, single C-O bonds in esters and anhydrides, and C-O bonds in carboxylic groups and/or water.

Finally, the deconvolution of the N1s high-resolution spectra was only possible for samples with surface nitrogen concentrations higher than 1 at. %. Curve fitting was not possible for the N1s high-resolution spectrum of H50S50T180_3 hydrochar, due to the low

area of the peak. N1s high-resolution spectra of both hydrochars and carbons exhibited three contributions assigned to three types of functional groups: N6, related to pyridinic nitrogen; N5, related to pyrrolic nitrogen; and NQ, assigned to quaternary nitrogen (Briggs, 2005; Dongil et al., 2011; Weidenthaler et al., 2006).

In general, pyrolysis decreased the relative concentrations of the groups related to CII and OII, while increasing the relative amounts of the groups related to the peaks CIII, CIV and OI. This finding means that the concentration of ethers, phenols, esters and anhydrides decreased whereas the concentration of quinone-type groups, carbonyls and carboxylic acids increased as a consequence of pyrolysis.

Concerning the structure of the carbons obtained by pyrolysis at 900°C of the aforementioned hydrochars, it can be added that none of these materials are graphitic, as evidenced by their XRD patterns showing very broad and poorly defined (002) and (10*l*) bands (see for instance (Tondi et al., 2009) and the supplementary information of (Celzard et al., 2019) for typical patterns of carbons based on tannin and tannin-sugar produced at 900°C). The corresponding Raman spectra demonstrated the same, but also that these materials are not graphitisable either, unless transition metals are added as graphitisation catalyst, which was not the case here. Typical Raman spectra of carbons based on tannin and tannin-sugar produced at 900°C can be found elsewhere (Celzard et al., 2019; Braghiroli et al., 2017), and prove that the present materials are definitely highly disordered, i.e. very poorly crystallised, carbons.

Concerning the morphology, carbon spheres have a wide range of applications, depending on their diameter, pore texture and surface chemistry. For example, they can be used in batteries (Park et al., 2018) or supercapacitors (Zhou et al., 2015), as catalysts (Frusteri et al., 2016, Maciá- Agulló et al., 2010) or even as boosters to produce pure water as we reported recently (Celzard et al., 2019).

393 Table 2. Atomic surface concentrations of C, N and O, and contributions to the C1s, O1s and N1s high-resolution XPS spectra of the materials in

394 terms of peak area fraction (%) at given binding energies (BE, eV).

Sample name	**Concentration** (at. %)			**C1s peak** BE (eV) Area (%)						**O1s peak** BE (eV) Area (%)			**N1s peak** BE (eV) Area (%)			
	C	**O**	**N**	**C***	**CI**	**CII**	**CIII**	**CIV**	**CV**	**O1**	**O2**	**O3**	**N6**	**N5**	**NQ**	**NX**
0S100T	80.4	19.6	-	-	284.4 66.1	285.8 29.6	288.2 2.5	289.2 0.9	291.0 0.9	531.7 24.8	532.8 75.2	-	-	-	-	-
H50S50T180_1	81.9	16.8	1.3	-	284.4 65.9	285.7 27.3	287.6 5.6	289.0 0.7	290.3 0.4	531.4 36.1	532.7 63.9	-	398.5 12.2	399.7 59.9	401.1 27.9	-
H50S50T180_2	83.0	15.7	1.3	-	284.4 73.7	285.8 19.4	287.6 4.6	288.9 1.9	290.6 0.4	531.4 41.7	532.7 58.3	-	398.5 28.1	399.7 58.5	401.1 13.4	-
H50S50T180_3	87.1	12.6	0.3	283.6 9.0	284.5 31.4	286.0 44.3	287.6 12.2	289.0 1.0	290.1 2.1	531.8 7.2	533.3 60.8	534.5 32.0	-	-	-	-
H50S50T180_u	84.2	15.8	-	-	284.4 73.7	285.7 20.7	287.6 3.7	289.0 1.6	290.3 0.3	531.7 39.5	532.8 60.5	-	-	-	-	-
H100S0T180_u	81.9	17.9	0.3	-	284.4 65.4	285.6 25.8	287.6 8.1	289.2 0.3	290.4 0.4	531.5 40.1	532.8 59.9	-	-	-	-	-
C0S100T	97.1	2.9	-	-	284.4 66.4	285.5 25.5	287.6 5.7	289.2 1.8	290.5 1.5	531.8 40.4	533.0 54.0	534.5 5.6	-	-	-	-
CH50S50T180_1	97.5	2.5	-	-	284.5 68.7	285.5 23.8	287.6 5.2	289.2 1.4	290.4 1.5	531.6 48.1	532.9 49.4	534.5 2.5	-	-	-	-
CH50S50T180_2	97.2	2.8	-	-	284.5 65.8	285.5 25.8	287.6 5.6	289.0 0.6	290.2 2.2	531.6 41.4	532.9 47.0	534.5 11.9	-	-	-	-
CH50S50T180_3	94.8	3.4	1.7	-	284.4 66.2	285.5 25.3	287.6 5.9	289.2 1.1	290.4 1.5	531.3 46.5	532.8 51.0	534.5 2.5	398.2 28.8	400.3 32.7	401.1 38.5	-
CH50S50T180_u	87.9	11.7	0.40	-	284.4 75.9	286.0 19.5	287.6 3.2	289.2 0.7	290.1 0.4	531.9 53.3	533.2 46.7	-	-	-	-	-
CH100S0T180_u	97.7	2.3	-	-	284.5 67.1	285.6 25.4	287.7 4.8	289.2 0.6	290.4 2.1	532.0 49.2	533.0 47.8	534.5 3.0	-	-	-	-

395

3.3 Electrochemical properties

Among the carbon materials, C0S100T, CH50S50T180_1 and CH50S50T180_u were selected for studying their electrochemical behaviour. With respect to porous texture, C0S100T and CH50S50T180_1 are among the materials having the highest micropore volumes, although their PSDs are clearly not the same, as suggested by the data of Table 1. With respect to surface chemistry, the most remarkable difference in their surface chemistry is that CH50S50T180_u exhibited higher surface oxygen content than the other two carbons, and that CH50S50T180_1 exhibited higher relative concentrations of quinone and carbonyl groups (OI peak). The latter are the most electroactive oxygen functionalities in acidic electrolytes (Inagaki et al., 2010). Choosing such materials for electrochemical tests was therefore supposed to clarify the understanding of these new carbon materials.

At the lowest scan rate of 0.5 mV s^{-1}, cyclic voltammetry (CV) curves of C0S100T and CH50S50T180_1 exhibited more defined peaks of both anodic and cathodic currents than CH50S50T180_u despite possessing a lower concentration of oxygen on their surfaces (Fig. 10a). The presence of redox peaks is due to a contribution of the surface oxygen groups to the total capacitance of the electrodes by a pseudocapacitance mechanism. Even at this low scan rate of 0.5 mV s^{-1}, CV curves of CH50S50T180_u exhibited a highly distorted profile with respect to the rectangular shape of an ideal electric-double layer capacitor (ELDC). This fact may indicate the existence of kinetic limitations for ion transport, and agrees with the highly microporous texture of the carbon, whose percentage of narrow porosity (width < 0.7 nm) was the highest of the three materials, 84.0%, and whose percentage of mesoporosity was the lowest one, 0.0%. At the relatively low scan rate of 10 mV s^{-1}, the shape of the CV curves of all the materials clearly deviated from the rectangular one, and no clear peak could be seen (Fig. 10b). This suggests that the behaviour of the supercapacitor electrodes becomes less

420 capacitive and more resistive, due to kinetic limitations, and that pseudocapacitance
421 contribution is negligible, respectively (McDonough et al., 2012).

422 The studied electrode materials yielded similar values of specific capacitance in the entire
423 range of investigated scan rates. At the lowest scan rate of 0.5 mV s^{-1}, specific capacitances of
424 51, 57 and 58 F g^{-1} were exhibited by C0S100T, CH50S50T180_1 and CH50S50T180_u,
425 respectively (Fig. 10c). These capacitance values progressively decreased when the scan rate
426 increased, due to the increasing resistance to diffusion of electrolyte ions into the pores. At
427 100 mV s^{-1} scan rate, the specific capacitance was 15 F g^{-1} for all the materials (Fig. 10c),
428 which corresponds to capacitance retentions of 30.4, 26.6 and 26.3% for C0S100T,
429 CH50S50T180_1 and CH50S50T180_u, respectively (Fig. 10d). The lower capacitance
430 retention of CH50S50T180_1 and CH50S50T180_u compared to C0S100T indicates the
431 existence of more important kinetic limitations at increasing scan rates due to their high
432 fractions of narrow porosity, 71.4 and 84.0%, respectively. The CV results agree with a
433 previous study on molasses-derived carbons, in which the materials prepared by HTC
434 exhibited, in the studied potential window, lower capacitances than those that were directly
435 pyrolysed, mainly due to their narrow porosities and low electrical conductivities (Sanchez-
436 Sanchez et al., 2016).

437 Figure 10

438 In order to determine the pseudocapacitance contribution to the overall capacitance of the
439 materials, interfacial capacitances at different scan rates, C / S_{NLDFT}, were plotted versus
440 oxygen surface concentrations (Fig. S7a of the Supporting Information section). The
441 interfacial capacitance was calculated by considering S_{NLDFT} instead of A_{BET}, since it has been
442 previously shown that this approach is more appropriate for materials mainly comprising
443 narrow pores, such as in the present case (Sanchez-Sanchez et al., 2016). In general, higher
444 surface oxygen concentrations were not related to higher interfacial capacitances in the entire

range of studied scan rates. This should mean that the pseudocapacitance contribution of the materials is lower than the capacitive contribution, for which the porous texture is the key parameter.

Oxygen functional groups have a great influence on the electrochemical properties of carbon materials (Anjos et al., 2013; Tanaka et al., 2015). Hydroxyl, carbonyl and, especially, quinone groups, have been proved to yield more capacitance than carboxyl, anhydride or lactone groups in acidic aqueous electrolytes thanks to their Faradaic reactions (Inagaki et al., 2010). Redox reactions involving these groups are the following (Oh et al., 2014):

Hydroxyls: $> C_xO + H^+ + e^- \leftrightarrow > C_xOH$

Carbonyls: $> C = O + H^+ + e^- \leftrightarrow > CH - O$

Quinones: 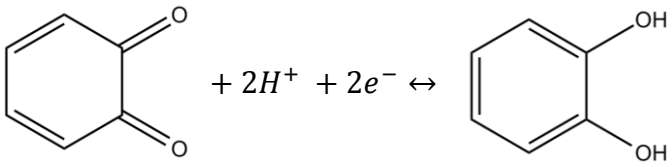

Carboxylic acids: $> COO^- + H^+ + e^- \leftrightarrow > COOH$

where the symbol > represents the surface of the carbon material. Protons, H^+, are not only simply adsorbed on the oxygen functional groups, but are involved in the electrochemical reactions.

As a consequence of these Faradaic reactions, redox peaks can appear on the anodic and cathodic branches of the CV curves of the carbon materials. CV curves obtained in a three-electrode cell in 1 mol L^{-1} H_2SO_4 electrolyte, measured at 0.5 mV s^{-1} scan rate and considering the first cycle of cycling, are displayed in Fig. 11. These curves exhibited two redox processes associated to peaks 1 and 2 appearing in the anodic and cathodic branches, which are represented by the “ox” and “red” superscript, and are defined by two parameters:

(i) peak current, I_p, which is the current at the maximum of the peak; and (ii) peak potential, E_p, which is the potential at the maximum of the peak (Fig. 11a, 11c and 11e).

Figure 11

For the samples C0S100T and CH50S50T180_1, no second anodic peak, $I_{p,2}^{ox}$, was seen, indicating the irreversibility of the associated redox process. In contrast, the first peak could be clearly observed both in the anodic and cathodic branches and appeared in the five cycles studied at scan rates from 0.5 to 5 mV s^{-1} for C0S100T, and from 0.5 to 2 mV s^{-1} for CH50S50T180_1 and CH50S50T180_u. This suggests that the associated redox system may be quasi-reversible in the aforementioned scan rate intervals. The highly distorted CV curves with respect to the expected rectangular shape of an ideal electric-double layer capacitor at scan rates above 2 or 5 mV s^{-1} did not allow differentiating clear redox peaks. Therefore, the reversibility of the redox system 1 was studied up to a maximum scan rate of 5 mV s^{-1}. The formal potentials of peak 1 vs SCE reference, calculated as $E^0 = 1/2\ (E_{p,1}^{ox} + E_{p,1}^{red})$, were 0.425, 0.424 and 0.444 V for C0S100T, CH50S50T180_1 and CH50S50T180_u, respectively. The reversible character of the redox process was evaluated through the following criteria:

1) *Peak separation, $\Delta E = E_{p,1}^{ox} - E_{p,1}^{red} \leq 0.059 / n$, where $E_{p,1}^{ox}$ and $E_{p,1}^{red}$ (V) are the maxima of the anodic and cathodic peaks, respectively, and n is the number of transferred electrons:* Considering the transfer of 1 electron, the peak separation was lower than 0.059 V at the lowest scan rate of 0.5 mV s^{-1} for the three materials, suggesting the reversibility of the redox process. ΔE generally increased above 0.059 V as the cycle number increased, which indicates that the redox process was progressively less reversible due to the gradual transformation of surface groups into non-electroactive species. However, ΔE was progressively lower than 0.059 V at the scan rate of 0.5 mV s^{-1} for the sample C0S100T, suggesting a higher reversibility of the redox process (Fig. 11b, 11d and 11f). This can be

explained by the improvement of the surface wettability during the cycling process, which facilitates the contact between the surface functionalities and the electrolyte ions, so that redox reactions are easier to occur, and also by the higher fraction of pores involved in the materials as the cycling process goes on (Jiang et al., 2013). Varying the scan rate in cyclic voltammetry allows varying the diffusion layer thickness, thus enabling the control of the electrochemical process either by electron transfer or by mass transport. The diffusion layer is thicker at low scan rates, and thinner as the scan rate increases. Electrochemical processes reflect the competition between reactions at the electrodes and diffusion, so that faster scan rates favour electrochemical irreversibility, which is controlled by the electron transfer rate, and the peak potentials are thus shifted. This trend is clearly observed in Fig. S7b of the Supporting Information section, which shows the progressive separation of maxima of the peaks associated to the redox process 1 at increasing scan rates from 0.5 to 2 mV s^{-1} for a representative sample, C0S100T (McDonough et al., 2012). When the peak potentials remain constant with increasing scan rates, the involved redox process is reversible. Fig. 12b, 12d and 12f show the progressive increase of the peak potentials of the studied samples, $E_p^{ox,red}$, at increasing scan rates, ln *s*, indicating the quasi-reversibility of the involved redox system (Gómez et al., 2011).

2) *Ratio of anodic to cathodic currents, $I_{p,1}^{ox} / I_{p,1}^{red} \approx 1$, where $I_{p,1}^{ox}$ and $I_{p,1}^{red}$ (A) are the currents at the maximum of the anodic and cathodic peaks, respectively:* When the peak currents, I_p, for the oxidation and reduction reactions are the same, i.e., $I_{p,1}^{ox} / I_{p,1}^{red} = 1$, the redox process is reversible (Bard and Faulkner, 2001). The current ratios of the studied samples at scan rates ranging from 0.5 to 2 mV s^{-1} were 0.98 ± 0.04, which indicates the quasi-reversibility of the redox process.

3) *Scan rate dependence of peak current, $I_p^{ox,red} \propto s^{1/2}$, where $I_p^{ox,red}$ (A) is the current at the maximum of the anodic or the cathodic peaks and $s^{1/2}$($V^{1/2}$ $s^{-1/2}$) is the square root of the*

scan rate: A linear relationship between $I_p^{ox,red}$ and $s^{1/2}$ indicates that the redox process is quasi-reversible (Gómez et al., 2011) As shown in Fig. 12a, 12b and 12c, $I_p^{ox,red}$ versus $s^{1/2}$ leads to linear relationships for the studied samples, with determination coefficients close to 1, thus indicating that the concerned redox processes are quasi-reversible. From these linear relationships and applying the Randles-Sevcik equation (Eq. 2), the diffusion coefficients, D_0, of the processes were calculated (McDonough et al., 2012). The Randles-Sevcik equation reads:

$$I_p = 0.4463\, n\, F\, A\, C\, [(F\, D_0\, s) / (R\, T)]^{1/2} \quad (2)$$

where I_p (A) is the peak current, n is the number of electrons transferred in the reaction, F (C mol^{-1}) is the Faraday constant, A (cm^2) is the electrode area, C (mol L^{-1}) is the concentration of the diffusing species in the bulk of the electrolyte, D_0 (cm^2 s^{-1}) is the corresponding diffusion coefficient, s (V s^{-1}) is the scan rate, R (J mol^{-1} K^{-1}) is the universal gas constant and T (K) is the temperature. Considering that n = 1 and C = 1 mol L^{-1} (H_2SO_4), the diffusion coefficients were found to be 1.602 × 10^{-13}, 1.156 × 10^{-13} and 6.973 × 10^{-14} cm^2 s^{-1} for C0S100T, C50S50T180_1 and C50S50T180_u, respectively. These values are considerably lower than those obtained for well-established redox processes in other doped carbons used as electrode materials, such as graphene-polyaniline (PANI) nanocomposites or PANI systems alone, suggesting a hindered ion transport (Gómez et al., 2011). Therefore, activation for opening the porosity and developing it further appears necessary for improving the electrochemical performance of these materials. For instance, we have recently shown that CO_2 activation allows increasing the surface area of tannin-derived mesoporous carbons up to nearly 2000 m^2/g and maintaining high-rate capability when increasing the current density up to 80 A/g (Castro-Gutiérrez et al., 2019). The same kind of behaviour can therefore be expected with the present samples.

Figure 12

4. Conclusions

Tannin-sucrose blends mixed in various proportions were submitted to hydrothermal carbonisation (HTC) at different pH and temperatures, and then pyrolysed at 900°C under nitrogen flow. Microporous carbon spheres with BET areas as high as 810 m^2/g, without further activation, were produced. Adding more sucrose produced microspheres of lower particle size due to the increased amount of germs produced by the HTC of sucrose.

HTC was confirmed to be an interesting low-cost and environment-friendly step to tune the properties of the resultant carbon materials, modifying their porous texture and their chemical composition, and thus broadening the range of their properties and therefore of their applications. The preliminary electrochemical tests reported here were carried out to select the most promising materials for further research. Although the carbon electrodes presented a quasi-reversible redox reaction concerning oxygen groups, their narrow pores hindered transport of electrolyte ions and led to low values of capacitance retention when increasing the current density and the scanning rate. Activation should significantly improve this results, and will be the object of a forthcoming study.

Acknowledgements

The present research was partly made possible by the support of the Region Lorraine and University of Lorraine through the programme ‘Jeunes chercheurs’. The French authors also gratefully acknowledge the financial support of the CPER 2007-2013 “Structuration du Pôle de Compétitivité Fibres Grand’Est” (Competitiveness Fibre Cluster), through local (Conseil Général des Vosges), regional (Région Lorraine), national (DRRT and FNADT) and European (FEDER) funds.

References

Anjos, D.M., McDonough, J.K., Perre, E., Brown, G.M., Overbury, S.H., Gogotsi, Y., Presser, V., 2013. Pseudocapacitance and performance stability of quinone-coated carbon onions. Nano Energy 2, 702–712. https://doi.org/10.1016/j.nanoen.2013.08.003

Antal, M.J., Mok, W.S.L., Richards, G.N., 1990. Mechanism of formation of 5-(hydroxymethyl)-2-furaldehyde from d-fructose and sucrose. Carbohydr. Res. 199, 91–109. https://doi.org/10.1016/0008-6215(90)84096-D

Antonietti, M., Titirici, M.-M., 2010. Coal from carbohydrates: The "chimie douce" of carbon. Comptes Rendus Chim. 13, 167–173. https://doi.org/10.1016/j.crci.2009.02.005

Asghari, F.S., Yoshida, H., 2006. Acid-catalyzed production of 5-hydroxymethyl furfural from d-fructose in subcritical water. Ind. Eng. Chem. Res. 45, 2163–2173. https://doi.org/10.1021/ie051088y

Bard, A.J., Faulkner, L.R., 2001. Electrochemical methods: fundamentals and applications, 2nd ed. ed. Wiley, New York.

Bate-Smith, E.C., 1962. The phenolic constituents of plants and their taxonomic significance. I. Dicotyledons. J. Linn. Soc. Lond. Bot. 58, 95–173. https://doi.org/10.1111/j.1095-8339.1962.tb00890.x

Braghiroli, F.L., Fierro, V., Izquierdo, M.T., Parmentier, J., Pizzi, A., Celzard, A., 2014. Kinetics of the hydrothermal treatment of tannin for producing carbonaceous microspheres. Bioresour. Technol. 151, 271–277. https://doi.org/10.1016/j.biortech.2013.10.045

Braghiroli, F.L., Fierro, V., Izquierdo, M.T., Parmentier, J., Pizzi, A., Celzard, A., 2012. Nitrogen-doped carbon materials produced from hydrothermally treated tannin. Carbon 50, 5411–5420. https://doi.org/10.1016/j.carbon.2012.07.027

Braghiroli, F.L., Fierro, V., Izquierdo, M.T., Parmentier, J., Pizzi, A., Delmotte, L., Fioux, P., Celzard, A., 2015a. High surface – highly N-doped carbons from hydrothermally treated tannin. Ind. Crops Prod. 66, 282–290. https://doi.org/10.1016/j.indcrop.2014.11.022

Braghiroli, F.L., Fierro, V., Parmentier, J., Vidal, L., Gadonneix, P., Celzard, A., 2015b. Hydrothermal carbons produced from tannin by modification of the reaction medium: Addition of H^+ and Ag^+. Ind. Crops Prod. 77, 364–374. https://doi.org/10.1016/j.indcrop.2015.09.010

Braghiroli, F.L., Fierro, V., Szczurek, A., Gadonneix, P., Ghanbaja, J., Parmentier, J., Medjahdi, G., Celzard, A., 2017. Hydrothermal Treatment of Tannin: A Route to Porous Metal Oxides and Metal/Carbon Hybrid Materials. Inorganics 5, 7. https://doi.org/10.3390/inorganics5010007

Briggs, D., 2005. Surface analysis of polymers by XPS and static SIMS, Cambridge solid state science series. Cambridge University Press, Cambridge ; New York.

Cagniant, D., Gruber, R., Boudou, J.P., Bilem, C., Bimer, J., Salbut, P.D., 1998. Structural characterization of nitrogen-enriched coals. Energy Fuels 12, 672–681. https://doi.org/10.1021/ef9700801

Castro-Gutiérrez, J., Diez, N., Sevilla, M., Izquierdo, M.T., Ghanbaja, J., Celzard, A., Fierro, V., 2019. High-Rate Capability of Supercapacitors Based on Tannin-Derived Ordered Mesoporous Carbons. ACS Sustainable Chem. Eng. 7, 17627−17635. https://doi.org/10.1021/acssuschemeng.9b03407

611 Celzard, A., Fierro, V., Amaral-Labat, G., Szczurek, A., Braghiroli, F.L., Parmentier, J., Pizzi,
612 A., Grishechko, L.I., Kuznetsov, B.N., 2012. Carbon gels derived from natural
613 resources. Bol. Grupo Esp. Carbón 26, 2–7.
614 Celzard, A., Pasc, A., Schaefer, S., Mandel, K., Ballweg, T., Li, S., Medjahdi, G., Nicolas, V.,
615 Fierro, V., 2019. Floating hollow carbon spheres for improved solar evaporation.
616 Carbon 146, 232–247. https://doi.org/10.1016/j.carbon.2019.01.101
617 Dongil, A.B., Bachiller-Baeza, B., Guerrero-Ruiz, A., Rodríguez-Ramos, I., Martínez-Alonso,
618 A., Tascón, J.M.D., 2011. Surface chemical modifications induced on high surface
619 area graphite and carbon nanofibers using different oxidation and functionalization
620 treatments. J. Colloid Interface Sci. 355, 179–189.
621 https://doi.org/10.1016/j.jcis.2010.11.066
622 Falco, C., Sevilla, M., White, R.J., Rothe, R., Titirici, M.-M., 2012. Renewable nitrogen-
623 doped hydrothermal carbons derived from microalgae. ChemSusChem 5, 1834–1840.
624 https://doi.org/10.1002/cssc.201200022
625 Figueiredo, J.L., Pereira, M.F.R., Freitas, M.M.A., Órfão, J.J.M., 1999. Modification of the
626 surface chemistry of activated carbons. Carbon 37, 1379–1389.
627 https://doi.org/10.1016/S0008-6223(98)00333-9
628 Gómez, H., Ram, M.K., Alvi, Farah., Villalba, P., Stefanakos, E. (Lee), Kumar, A., 2011.
629 Graphene-conducting polymer nanocomposite as novel electrode for supercapacitors.
630 J. Power Sources 196, 4102–4108. https://doi.org/10.1016/j.jpowsour.2010.11.002
631 Frusteri, L., Cannilla, C., Bonura, G., Chuvilin, A.L., Perathoner, S., Centi, G., Frusteri, F.,
632 2016. Carbon microspheres preparation, graphitization and surface functionalization
633 for glycerol etherification. Catal. Today 277, 66-77.
634 https://doi.org/10.1016/j.cattod.2016.02.044
635 Hemingway, R.W., Karchesy, J.J., Branham, S.J. (Eds.), 1989. Chemistry and Significance of
636 Condensed Tannins. Springer US, Boston, MA. https://doi.org/10.1007/978-1-4684-
637 7511-1
638 Hu, B., Wang, K., Wu, L., Yu, S.-H., Antonietti, M., Titirici, M.-M., 2010. Engineering
639 carbon materials from the hydrothermal carbonization process of biomass. Adv.
640 Mater. 22, 813–828. https://doi.org/10.1002/adma.200902812
641 Inagaki, M., Konno, H., Tanaike, O., 2010. Carbon materials for electrochemical capacitors.
642 J. Power Sources 195, 7880–7903. https://doi.org/10.1016/j.jpowsour.2010.06.036
643 Jiang, J., Zhang, L., Wang, X., Holm, N., Rajagopalan, K., Chen, F., Ma, S., 2013. Highly
644 ordered macroporous woody biochar with ultra-high carbon content as supercapacitor
645 electrodes. Electrochimica Acta 113, 481–489.
646 https://doi.org/10.1016/j.electacta.2013.09.121
647 Kabyemela, B.M., Adschiri, T., Malaluan, R.M., Arai, K., 1997. Kinetics of glucose
648 epimerization and decomposition in subcritical and supercritical water. Ind. Eng.
649 Chem. Res. 36, 1552–1558. https://doi.org/10.1021/ie960250h
650 Kim, J.S., Lee, Y.Y., Torget, R.W., 2001. Cellulose hydrolysis under extremely low sulfuric
651 acid and high-temperature conditions. Appl. Biochem. Biotechnol. 91–93, 331–340.
652 Lee, Y.Y., Iyer, Prashant, Torget, R.W., 1999. Dilute-Acid Hydrolysis of Lignocellulosic
653 Biomass, in: Tsao, G.T., Brainard, A.P., Bungay, H.R., Cao, N.J., Cen, P., Chen, Z.,
654 Du, J., Foody, B., Gong, C.S., Hall, P., Ho, N.W.Y., Irwin, D.C., Iyer, P., Jeffries,
655 T.W., Ladisch, C.M., Ladisch, M.R., Lee, Y.Y., Mosier, N.S., Mühlemann, H.M.,
656 Sedlak, M., Shi, N.-Q., Tsao, G.T., Tolan, J.S., Torget, R.W., Wilson, D.B., Xia, L.
657 (Eds.), Recent Progress in Bioconversion of Lignocellulosics. Springer Berlin
658 Heidelberg, Berlin, Heidelberg, pp. 93–115. https://doi.org/10.1007/3-540-49194-5_5

659 Letellier, M., Szczurek, A., Basso, M.-C., Pizzi, A., Fierro, V., Ferry, O., Celzard, A., 2017.
660 Preparation and structural characterisation of model cellular vitreous carbon foams.
661 Carbon 112, 208–218. https://doi.org/10.1016/j.carbon.2016.11.017
662 Luijkx, G.C., van Rantwijk, F., van Bekkum, H., Antal, M.J., 1995. The role of deoxyhexonic
663 acids in the hydrothermal decarboxylation of carbohydrates. Carbohydr. Res. 272,
664 191–202.
665 Maciá-Agulló, J.A., Sevilla, M., Diez, M.A., Fuertes, A.B., 2010. Synthesis of Carbon- based
666 Solid Acid Microspheres and Their Application to the Production of Biodiesel.
667 ChemSusChem 3, 1352-1354. https://doi.org/10.1002/cssc.201000308
668 McDonough, J.K., Frolov, A.I., Presser, V., Niu, J., Miller, C.H., Ubieto, T., Fedorov, M.V.,
669 Gogotsi, Y., 2012. Influence of the structure of carbon onions on their electrochemical
670 performance in supercapacitor electrodes. Carbon 50, 3298–3309.
671 https://doi.org/10.1016/j.carbon.2011.12.022
672 Oh, Y.J., Yoo, J.J., Kim, Y.I., Yoon, J.K., Yoon, H.N., Kim, J.-H., Park, S.B., 2014. Oxygen
673 functional groups and electrochemical capacitive behavior of incompletely reduced
674 graphene oxides as a thin-film electrode of supercapacitor. Electrochimica Acta 116,
675 118–128. https://doi.org/10.1016/j.electacta.2013.11.040
676 Park, G.D., Kim, J.H., Lee, J.K., Kang, Y.C., 2018. Carbon microspheres with well-developed
677 micro- and mesopores as excellent selenium host materials for lithium–selenium
678 batteries with superior performances. J Mat Chem A 6, 21410-21418.
679 https://doi.org/10.1039/C8TA08727J
680 Pizzi, A., 1994. Advanced wood adhesives technology. M. Dekker, New York.
681 Pizzi, A., 1983. Tannin-based wood adhesives, in: Pizzi, A. (Ed.), Wood Adhesives:
682 Chemistry and Technology. Marcel Dekker, New York, pp. 177–246.
683 Sanchez-Sanchez, A., Izquierdo, M.T., Medjahdi, G., Ghanbaja, J., Celzard, A., Fierro, V.,
684 2018. Ordered mesoporous carbons obtained by soft-templating of tannin in mild
685 conditions. Microporous Mesoporous Mater. 270, 127–139.
686 https://doi.org/10.1016/j.micromeso.2018.05.017
687 Sanchez-Sanchez, A., Martinez de Yuso, A., Braghiroli, F.L., Izquierdo, M.T., Alvarez, E.D.,
688 Pérez-Cappe, E., Mosqueda, Y., Fierro, V., Celzard, A., 2016. Sugarcane molasses as
689 a pseudocapacitive material for supercapacitors. RSC Adv 6, 88826–88836.
690 https://doi.org/10.1039/C6RA16314A
691 Schaefer, S., Fierro, V., Izquierdo, M.T., Celzard, A., 2016. Assessment of hydrogen storage
692 in activated carbons produced from hydrothermally treated organic materials. Int. J.
693 Hydrog. Energy 41, 12146–12156. https://doi.org/10.1016/j.ijhydene.2016.05.086
694 Sevilla, M., Fuertes, A.B., 2009. Chemical and structural properties of carbonaceous products
695 obtained by hydrothermal carbonization of saccharides. Chem. - Eur. J. 15, 4195–
696 4203. https://doi.org/10.1002/chem.200802097
697 Szczurek, A., Amaral-Labat, G., Fierro, V., Pizzi, A., Celzard, A., 2011a. The use of tannin to
698 prepare carbon gels. Part II. Carbon cryogels. Carbon 49, 2785–2794.
699 https://doi.org/10.1016/j.carbon.2011.03.005
700 Szczurek, A., Amaral-Labat, G., Fierro, V., Pizzi, A., Masson, E., Celzard, A., 2011b. The use
701 of tannin to prepare carbon gels. Part I: Carbon aerogels. Carbon 49, 2773–2784.
702 https://doi.org/10.1016/j.carbon.2011.03.007
703 Tanaka, S., Fujimoto, H., Denayer, J.F.M., Miyamoto, M., Oumi, Y., Miyake, Y., 2015.
704 Surface modification of soft-templated ordered mesoporous carbon for
705 electrochemical supercapacitors. Microporous Mesoporous Mater. 217, 141–149.
706 https://doi.org/10.1016/j.micromeso.2015.06.017
707 Tellez-Juárez, M.C., Fierro, V., Zhao, W., Fernández-Huerta, N., Izquierdo, M.T., Reguera,
708 E., Celzard, A., 2014. Hydrogen storage in activated carbons produced from coals of

different ranks: Effect of oxygen content. Int. J. Hydrog. Energy 39, 4996–5002. https://doi.org/10.1016/j.ijhydene.2014.01.071
Titirici, M.-M., Antonietti, M., Baccile, N., 2008. Hydrothermal carbon from biomass: a comparison of the local structure from poly- to monosaccharides and pentoses/hexoses. Green Chem. 10, 1204. https://doi.org/10.1039/b807009a
Titirici, M.M., Thomas, A., Yu, S.-H., Müller, J.-O., Antonietti, M., 2007. A direct synthesis of mesoporous carbons with bicontinuous pore morphology from crude plant material by hydrothermal carbonization. Chem. Mater. 19, 4205–4212. https://doi.org/10.1021/cm0707408
Tondi, G., Zhao, W., Pizzi, A., Du, G., Fierro, V., Celzard, A., 2009. Tannin-based rigid foams: A survey of chemical and physical properties. Bioresour. Technol. 100, 5162–5169. https://doi.org/10.1016/j.biortech.2009.05.055
Trajano, H.L., Wyman, C.E., 2013. Fundamentals of Biomass Pretreatment at Low pH, in: Wyman, C.E. (Ed.), Aqueous Pretreatment of Plant Biomass for Biological and Chemical Conversion to Fuels and Chemicals. John Wiley & Sons, Ltd, Chichester, UK, pp. 103–128. https://doi.org/10.1002/9780470975831.ch6
Ulbricht, R., 1984. A review of 5-hydroxymethylfurfural (HMF) in parenteral solutions. Fundam. Appl. Toxicol. 4, 843–853. https://doi.org/10.1016/0272-0590(84)90106-4
Unur, E., 2013. Functional nanoporous carbons from hydrothermally treated biomass for environmental purification. Microporous Mesoporous Mater. 168, 92–101. https://doi.org/10.1016/j.micromeso.2012.09.027
van Krevelen, D.W., 1950. Graphical-statistical method for the study of structure and reaction processes of coal. Fuel 29, 269–284.
Wang, Q., Li, H., Chen, L., Huang, X., 2001. Monodispersed hard carbon spherules with uniform nanopores. Carbon 39, 2211–2214. https://doi.org/10.1016/S0008-6223(01)00040-9
Weckhuysen, B.M., Rosynek, M.P., Lunsford, J.H., 1998. Characterization of surface carbon formed during the conversion of methane to benzene over Mo/H-ZSM-5 catalysts. Catal. Lett. 52, 31–36.
Weidenthaler, C., Lu, A.-H., Schmidt, W., Schüth, F., 2006. X-ray photoelectron spectroscopic studies of PAN-based ordered mesoporous carbons (OMC). Microporous Mesoporous Mater. 88, 238–243. https://doi.org/10.1016/j.micromeso.2005.09.015
White, R.J., Antonietti, M., Titirici, M.-M., 2009. Naturally inspired nitrogen doped porous carbon. J. Mater. Chem. 19, 8645. https://doi.org/10.1039/b911528e
Zhao, L., Baccile, N., Gross, S., Zhang, Y., Wei, W., Sun, Y., Antonietti, M., Titirici, M.-M., 2010. Sustainable nitrogen-doped carbonaceous materials from biomass derivatives. Carbon 48, 3778–3787. https://doi.org/10.1016/j.carbon.2010.06.040
Zhao, Y., Li, W., Zhao, X., Wang, D.P., Liu, S.X., 2013. Carbon spheres obtained via citric acid catalysed hydrothermal carbonisation of cellulose. Mater. Res. Innov. 17, 546–551. https://doi.org/10.1179/1433075X13Y.0000000108
Zhou, J., Lian, J., Hou, L., Zhang, J., Gou, H., Xia, M., Zhao, Y., Strobel, T.A., Tao, L., Gao, F., 2015. Ultrahigh volumetric capacitance and cyclic stability of fluorine and nitrogen co-doped carbon microspheres. Nat. Comm., 6, 8503. https://doi.org/10.1038/ncomms9503

Captions of the Figures

Fig. 1: Main flavonoid unit contained in Mimosa tannin extract.

Fig. 2: Changes of HTC yield of H0S100T180 and H50S50T180 hydrochars obtained at different pH, and BET areas of the corresponding carbons after subsequent pyrolysis at 900°C (dashed lines are just guides for the eye).

Fig.3: Typical SEM images of carbon materials (i.e., pyrolysed at 900°C) based on: tannin (CH0S100T) and sucrose (CH100S0T) submitted to HTC at 180°C with, a) and b) unmodified pH and d) and e) pH 2, respectively; based on 50S50T samples submitted to HTC at 180°C with c) unmodified pH and f) pH 2; and finally based on 50S50T samples submitted to HTC at pH 2 g) at 160°C and h) 200°C.

Fig. 4: Total carbon yield and BET area of HTC materials (H50S50T) prepared at different HTC temperatures (160, 180 and 200°C) at unmodified pH and pH 2, and of pyrolysed (900°C) CH50S50T carbons.

Fig. 5: Typical SEM images of carbon materials (i.e., pyrolysed at 900°C) based on sucrose and tannin mixed in proportions ranging from 25-75 to 100-0 (from left to right) and submitted to HTC at unmodified pH (a, b, c) and pH 2 (d, e, f).

Fig. 6: a) HTC yield of materials made at 180°C at different T/S proportions and of CH50S50T samples prepared at 160 and 200°C; b) Corresponding BET areas A_{BET} after HTC and subsequent pyrolysis at 900°C. The dashed lines in a) were calculated (see text), and are just guides for the eye in b).

Fig. 7: BET areas A_{BET} (open symbols) and product Total carbon yield × A_{BET} (full symbols) as a function of the total carbon yield for materials at different T/S proportions after HTC at 180°C and subsequent pyrolysis at 900°C.

Fig. 8: a) Nitrogen adsorption-desorption isotherms (full and open symbols, respectively) at -196°C for CH50S50T180_2 and CH50S50T180_u samples; and b) their pore size distributions determined by the DFT method (slit-like pore geometry).

Fig. 9: a) Van Krevelen diagram for all materials before (100S0T and 0S100T) and after HTC (H100S0T and H0S100T) at 160, 180 and 200°C, at unmodified pH (HsStT_u) and at pH 2 (HsStT_2) and posterior pyrolysis at 900°C (HTC_900°C); and b) total amounts of CO and CO_2 gases produced during TPD analysis for materials after HTC at 180°C at different weight fractions of tannin.

Figure 10. Cyclic voltammetry (CV) results obtained in a three-electrode cell in 1 mol L^{-1} H_2SO_4 electrolyte: (a) CV curves recorded at 0.5 mV s^{-1} scan rate; (b) CV curves recorded at 10 mV s^{-1} scan rate; (c) Specific capacitance of the samples at scan rates between 0.5 and 100 mV s^{-1}; (d) Capacitance retention at scan rates between 0.5 and 100 mV s^{-1}.

Figure 11. Cyclic voltammetry (CV) results obtained in a three-electrode cell in 1 mol L^{-1} H_2SO_4 electrolyte: (a, c, e) CV curves recorded at 0.5 mV s^{-1} scan rate for the first cycle, showing the redox peaks on both anodic and cathodic branches; (b, d, f) Evolution of the potential difference (ΔE) between the maxima of the anodic and cathodic peak 1 as a function of the cycle number; CV curves were recorded at scan rates between 0.5 and 5 mV s^{-1} for C0S100T, and between 0.5 and 2 mV s^{-1} for CH50S50T180_1 and CH50S50T180_u.

Figure 12. (a, c, e) Dependence of the anodic and cathodic peaks currents, $I_{p,ox}$ and $I_{p,red}$, on the square root of the scan rate, $s^{1/2}$; (b, d, f) Evolution of the peak potentials, $E_{p,ox}$ and $E_{p,red}$, versus the natural logarithm of the scan rate, ln s.

804 Synthesis and properties of porous carbons based on tannin-sucrose mixtures treated in
805 hydrothermal conditions
806 Sanchez-Sanchez et al.

807

808

809 Figure 1

810

811

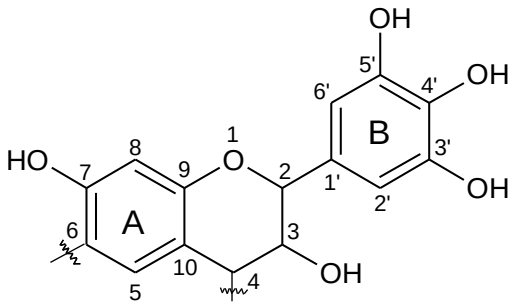

812

813

817

818

819 Figure 2

820

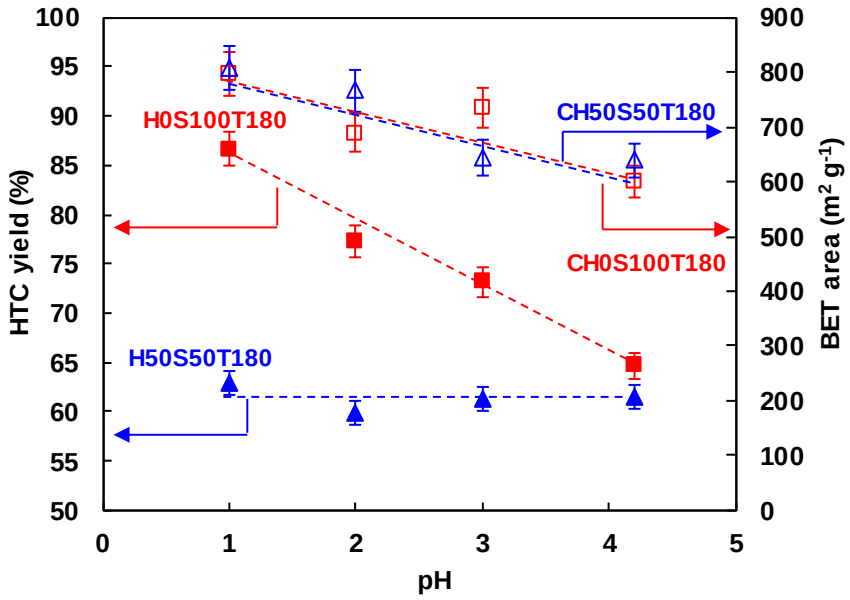

821

822

Synthesis and properties of porous carbons based on tannin-sucrose mixtures treated in hydrothermal conditions

Sanchez-Sanchez et al.

Figure 3

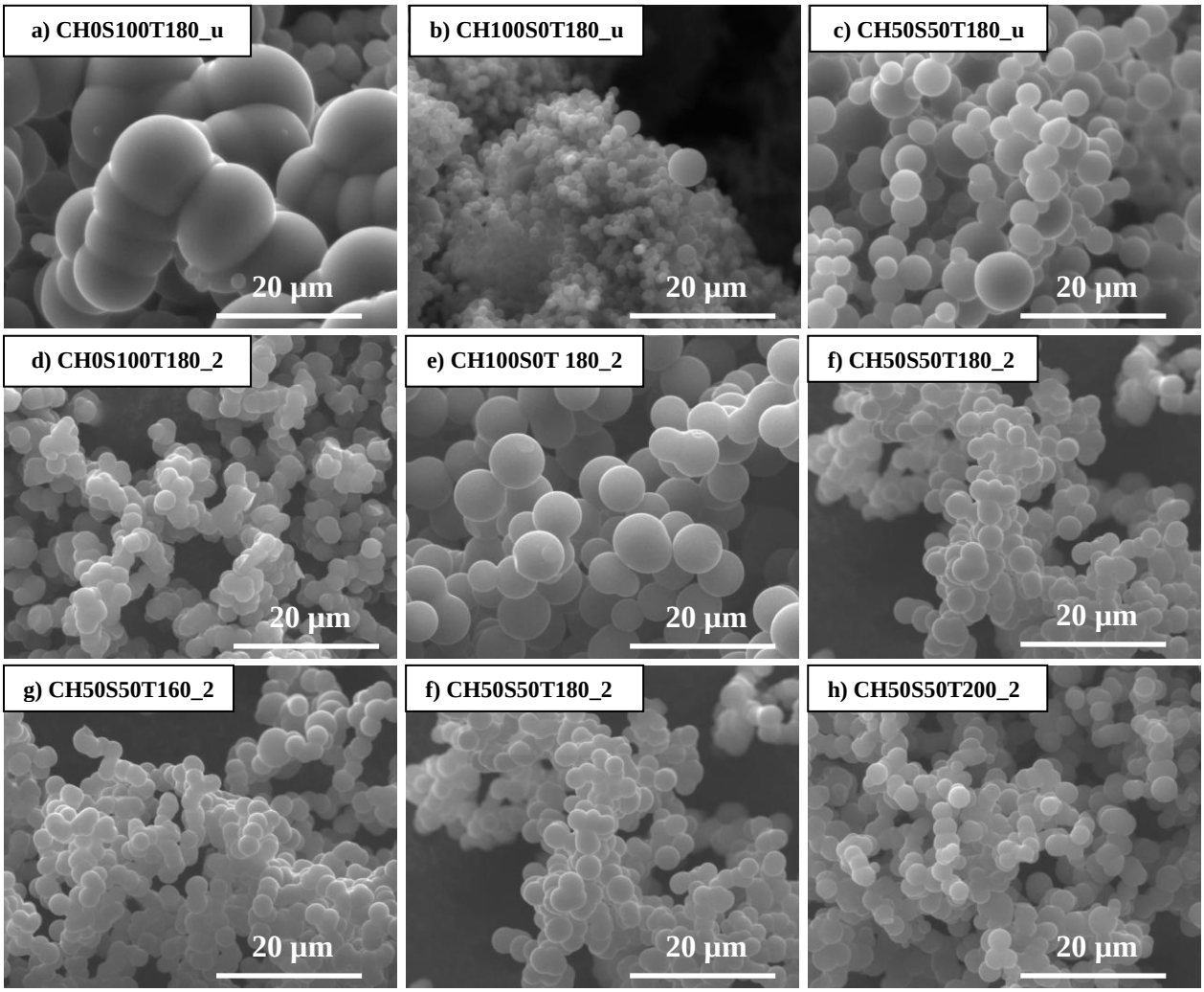

Figure 4

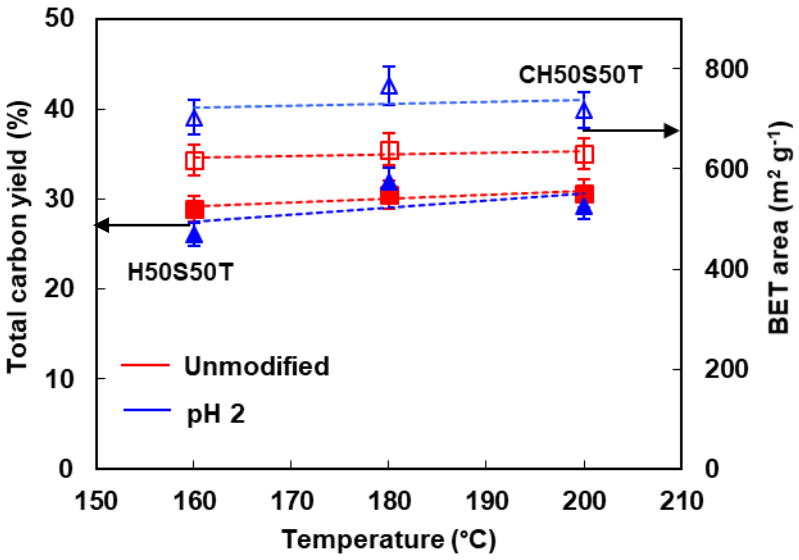
Total carbon yield (%)
BET area (m² g⁻¹)
Temperature (°C)
CH50S50T
H50S50T
Unmodified
pH 2
0
10
20
30
40
50
0
200
400
600
800
150
160
170
180
190
200
210

Synthesis and properties of porous carbons based on tannin-sucrose mixtures treated in hydrothermal conditions

Sanchez-Sanchez et al.

Figure 5

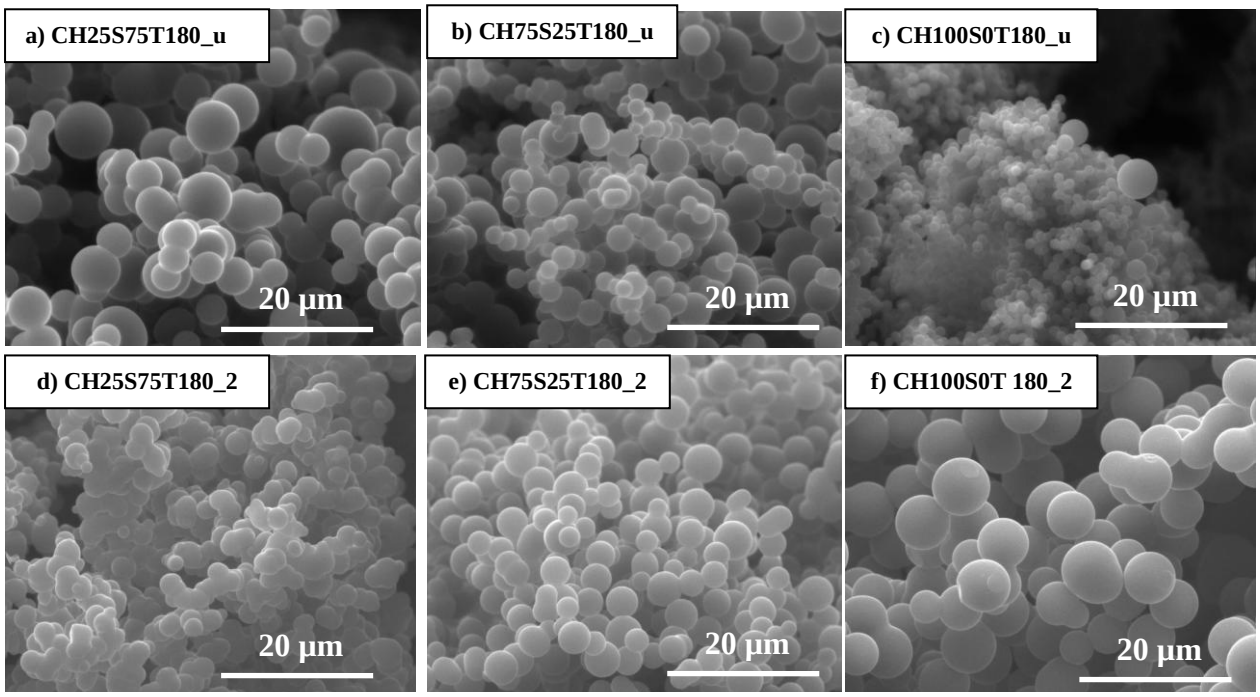

Synthesis and properties of porous carbons based on tannin-sucrose mixtures treated in hydrothermal conditions

Sanchez-Sanchez et al.

Figure 6

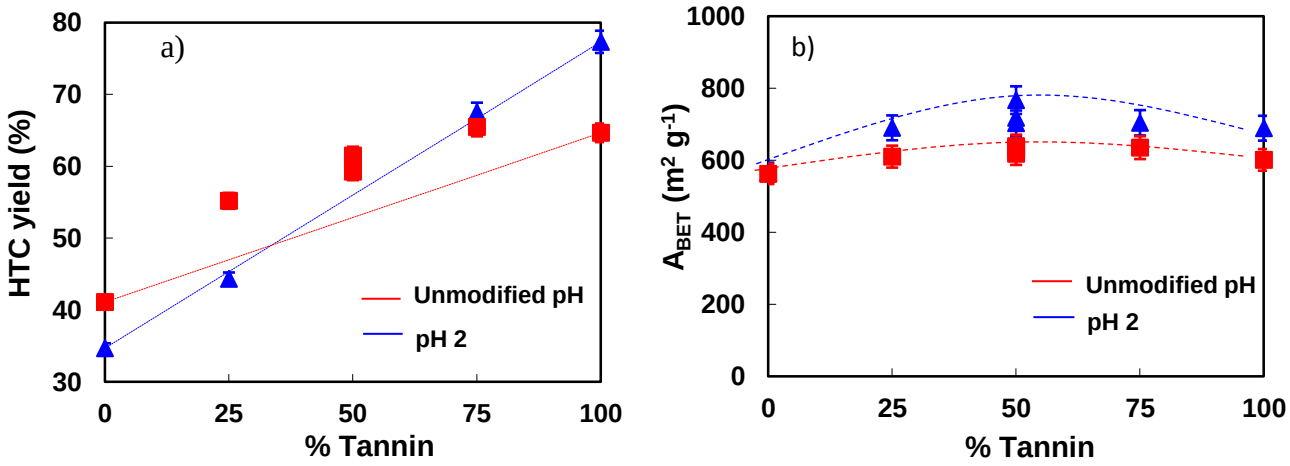

866 Synthesis and properties of porous carbons based on tannin-sucrose mixtures treated in
867 hydrothermal conditions
868 Sanchez-Sanchez et al.

869

870

871 Figure 7

872

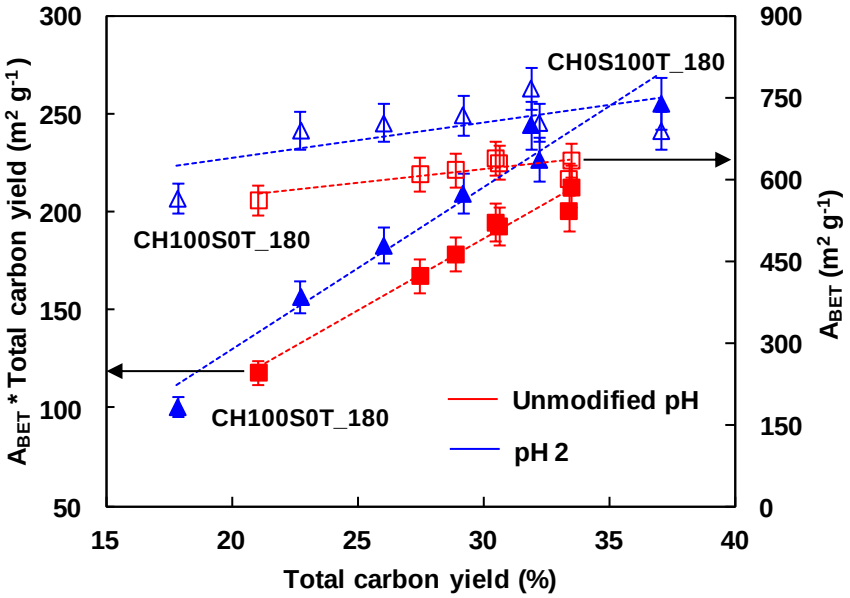

873

874

875 Synthesis and properties of porous carbons based on tannin-sucrose mixtures treated in
876 hydrothermal conditions
877 Sanchez-Sanchez et al.

878

879

880 Figure 8

881

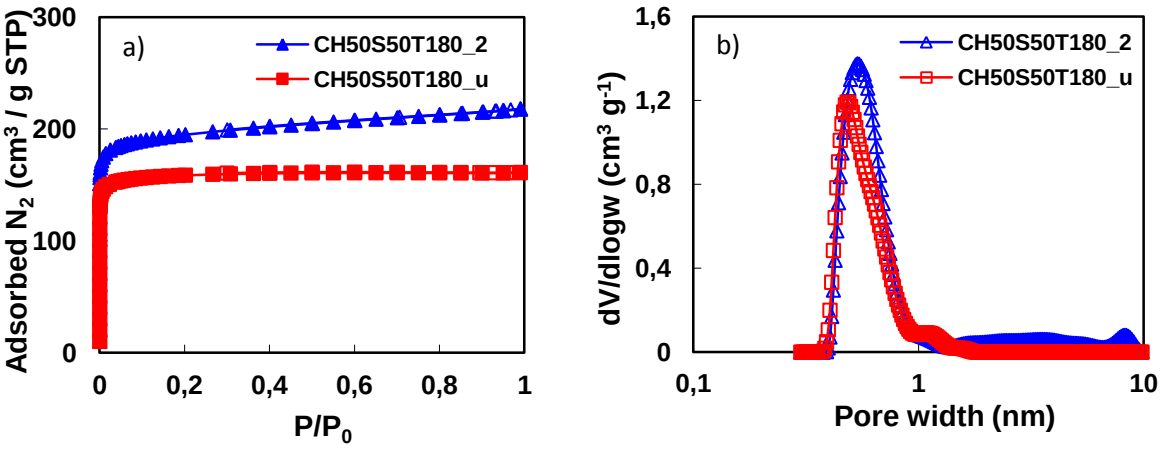

882

883

884 Synthesis and properties of porous carbons based on tannin-sucrose mixtures treated in
885 hydrothermal conditions
886 Sanchez-Sanchez et al.

887

888

889 Figure 9

890

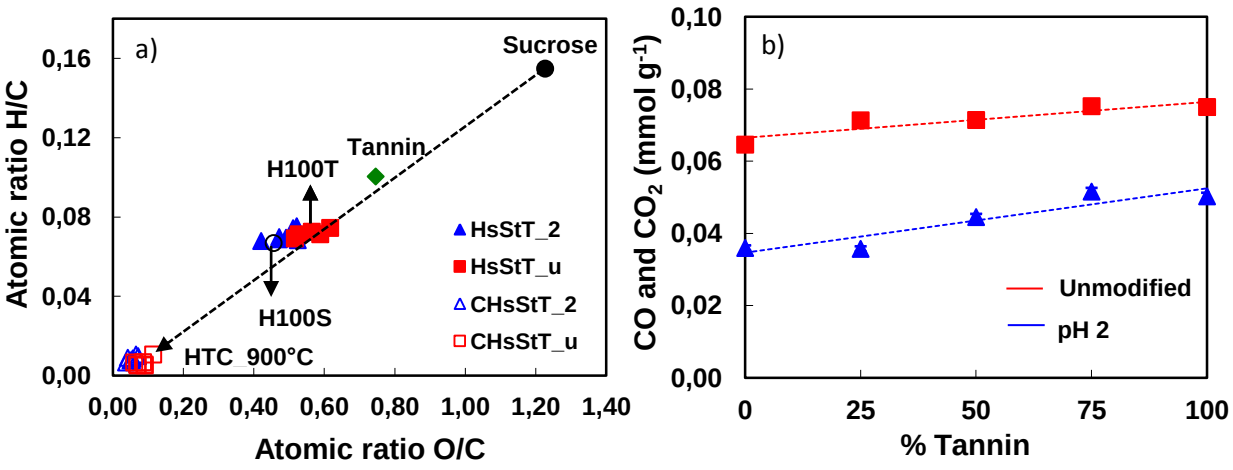

891

892

896

897

898 Figure 10

899

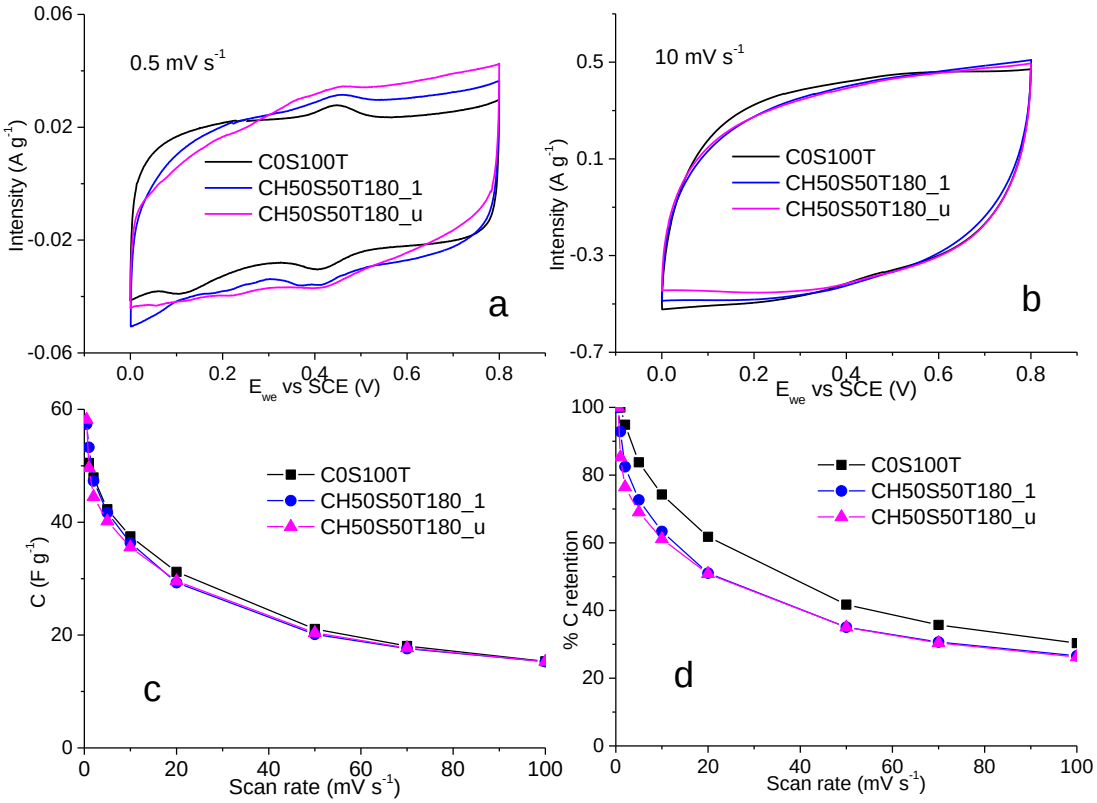

900

901

902

903

907

908 Figure 11

909

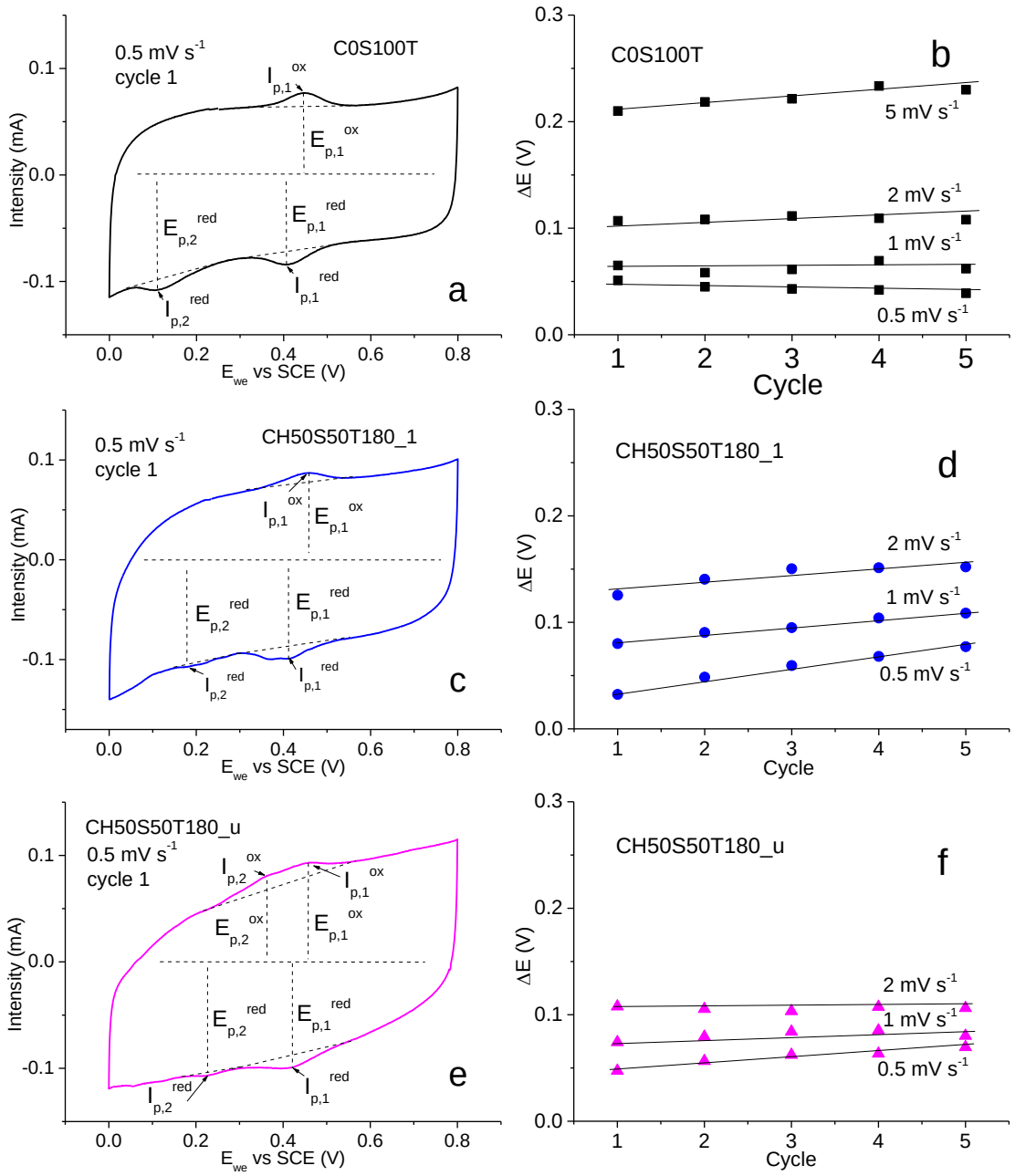

910
911

Synthesis and properties of porous carbons based on tannin-sucrose mixtures treated in hydrothermal conditions

Sanchez-Sanchez et al.

Figure 12